Journal of Marine Science and Technology

Volume 25 | Issue 1 Article 5

INTELLIGENT DETECTION OF SERIAL ARC FAULT ON LOW VOLTAGE POWER LINES

Chi-Jui Wu
Department of Electrical Engineering, National Taiwan University of Science and Technology, Taipei County, Taiwan, R.O.C.

Yu-Wei Liu
Department of Electrical Engineering, National Taiwan University of Science and Technology, Taipei County, Taiwan, R.O.C., d9907102@mail.ntust.edu.tw

Chen-Shung Hung
Department of Electrical Engineering, National Taiwan University of Science and Technology, Taipei County, Taiwan, R.O.C.

Journal of Marine Science and Technology, Vol. 25, No. 1, pp. 43-53 (2017)
DOI: 10.6119/JMST-016-1116-1

INTELLIGENT DETECTION OF SERIAL ARC FAULT ON LOW VOLTAGE POWER LINES

Chi-Jui Wu, Yu-Wei Liu, and Chen-Shung Hung

Key words: serial arc fault detection, low voltage power line, discrete wavelet transform, back propagation neural network.

ABSTRACT

Some reports reveal that a number of home fires are caused by electric arc faults on low voltage electric power lines. The arc fault circuit interrupter (AFCI) is a device to detect arc faults. However, the accurate rate of detection by commercial AFCIs is still imperfect. In this paper, an intelligent method is intended to improve the detection ability. A wavelet based stationary non-stationary filter (WTST-NST) is employed to eliminate the impulse components of measurement data. Then, the discrete wavelet transform (DWT) and the multi-resolution are used to obtain the signal energy in the corresponding frequency band. A back propagation neural network (BPNN) is trained by using the signal energy. After the training procedure, the BPNN is able to detect the occurrence of serial arc faults. Finally, the detection results of the system under several loading conditions and operation conditions are compared with a commercial AFCI.

I. INTRODUCTION

A certain percentage of home fires is caused by unsafe use of electricity. For using electric power safely, it is important to detect overload or leakage conditions on low voltage power lines by using some protection devices such as magnetic circuit breakers or leakage current breakers. However, arc faults on low voltage electrical power lines is also an important factor to cause fire events (Gregory and Scott, 1998; Hall, 2013). The serial arc faults occur more often than parallel arc faults (Muller et al., 2010). The arc fault circuit interrupter (AFCI) is intended to mitigate the effects of arc faults that may cause risks of fire (Arch-fault circuit interrupters, 2008; Lippert and Domitrovich, 2013). The signal detection circuit is important in designing an AFCI. However, the ability of an AFCI to perform correctly still needs to be improved (Su and Wu, 2010).

Paper submitted 04/08/14; revised 01/15/16; accepted 11/16/16. Author for correspondence: Yu-Wei Liu (e-mail: d9907102@mail.ntust.edu.tw).
Department of Electrical Engineering, National Taiwan University of Science and Technology, Taipei County, Taiwan, R.O.C.

There are many studies for arc fault detection (Kim et al., 2002; Lin et al., 2004; Naidu et al., 2006; Zhang and Song, 2012; Koziy et al., 2013). They detect whether arc faults occur or not by grabbing some characteristics from voltage or current in a power line and then comparing the characteristics with a threshold value (Lin et al., 2004; Naidu et al., 2006). In some studies (Kim et al., 2002; Zhang and Song, 2012; Koziy et al., 2013), they obtain the adaptive frequency components from voltage or current in a power line and then compare the components with a threshold to detect arc faults. For instances, the signal of adaptive frequency band can be extracted from current data in power line and compared the maximum magnitude with a threshold value (Zhang and Song, 2012). The summation of the absolute value which is analyzed by using the discrete wavelet transform (DWT) is used to compare with a threshold (Kim et al., 2002). The signal components within 2 to 4-kHz can be obtained from current data and then compared with a threshold (Koziy et al., 2013). However, different low voltage electrical appliances have different characteristics, and thus, the threshold is hard to determine.

This study employs the wavelet based stationary non-stationary filter (WTST-NST) to remove the impulse components of measurement data of the current on the power lines (Hadjileontiadis and Panas, 1997). Then, the resulted data are treated by the multi-resolution analysis based on DWT to obtain sub-band components. The load characteristics can be reflected by the signal energy of sub-band components. Then the values of signal energy are used to train the back propagation neural network (BPNN) (Abedi, 2010; Ma and Guan, 2011). The BPNN has three layers, input, hidden, and output. This study uses a simpler structure which has only one hidden layer in the BPNN. From the test results, the purposed method in this paper can identify correctly the occurrence of serial arc faults.

II. CHARACTERISTICS OF SERIAL ARC FAULT ON LOW VOLTAGE POWER LINES

Arc faults can be divided into parallel and serial faults. Because parallel arc faults have conspicuous fault currents and are similar to short circuit faults (Muller et al., 2010), so that they can be detected easily. However, the fault currents of serial arc faults are usually unnoticed, therefore, it is more difficult to detect them. Fig. 1 gives a single line diagram of an indoor

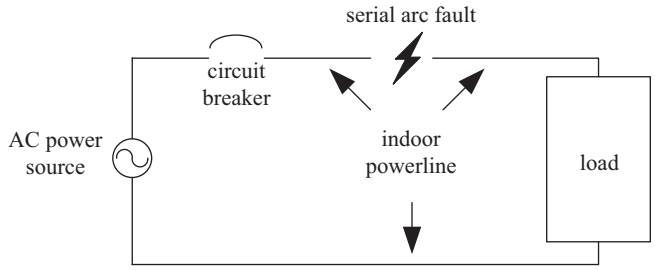

Fig. 1. Schematic diagram of an indoor power line with serial arc fault.

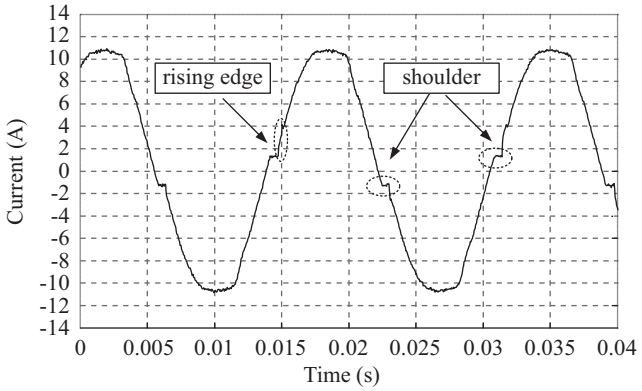

Fig. 2. Current waveform of a power line feeding a hairdryer under serial arc fault.

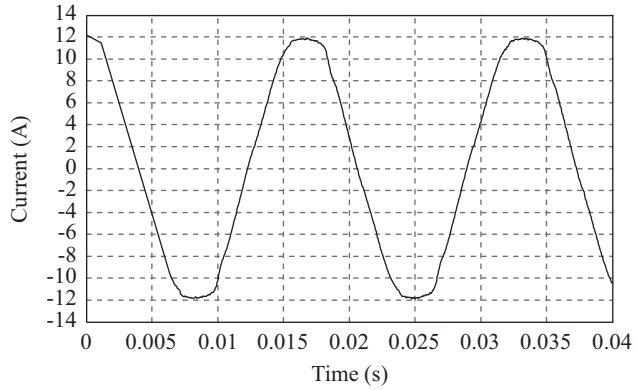

Fig. 3. Current waveform of a power line feeding a hairdryer under normal operation.

power line with a serial arc fault, which might occur when there is a gap on the conductors. Since the serial arc is series connection with the load, it will limit the fault current (Fig. 1). Consequently, it is hard to detect serial arc faults by using the traditional over current protection devices. For this reason, the characteristics of serial arc faults in time domain and frequency domain should be well studied to develop the detection technology.

1. Time Domain Characteristics

The line current waveform in Fig. 2 can be used to reveal the time-domain characteristics of serial arc faults (Gregory and Scott, 1998; Muller et al., 2010):

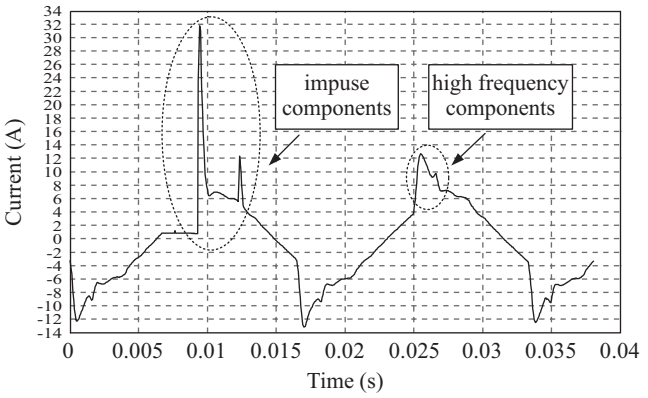

Fig. 4. Current waveform of a power line feeding fluorescent lamps and a parallel resistor under serial arc fault.

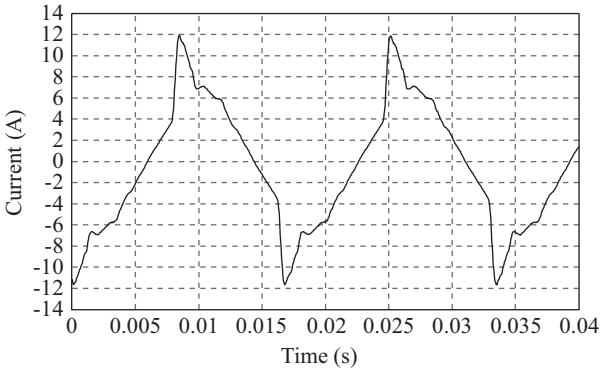

Fig. 5. Current waveform of a power line feeding fluorescent lamps and a parallel resistor under normal operation.

(1) When a serial arc fault happens, the current waveform has shoulder phenomenon, which means that a flat shape is generated when the current is crossing the zero ampere (Fig. 2). Therefore, the shoulder occurs every half-cycle.
(2) After the shoulder interval, the increasing rate of the current is greater than that under normal operation. A precipitous rising edge appears after the shoulder.
(3) An equivalent impedance is introduced by the serial arc to increase the equivalent impedance of the power line. Thus, the root mean square value of the current on the power line is smaller than that under normal operation, by comparing Figs. 2 and 3.

2. Frequency Domain Characteristics

Several characteristics of serial arc faults in the frequency domain also have been investigated in (Muller et al., 2010) and (Cheng et al., 2010):

(1) Since the precipitous rising edge after the shoulder is about 10 μs to 100 μs, the frequency components are between 2 and 5 kHz.
(2) The serial arc faults introduce higher frequency components. By observing Figs. 4 and 5, there are impulse and higher frequency components within line current when a serial arc fault happens.

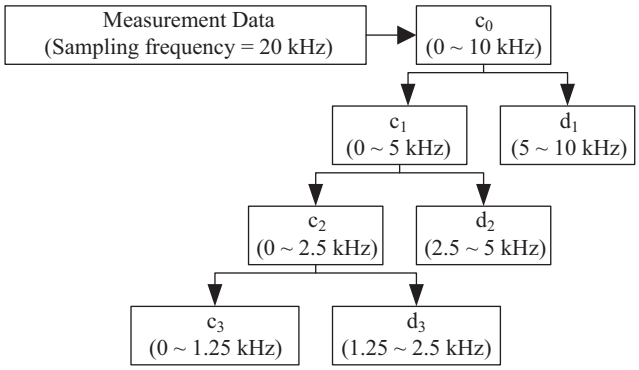

Fig. 6. A three-layer resolution of a signal by using DWT.

III. SIGNAL ANALYSYS BY USING WAVELET

1. Wavelet Transform

The wavelet transform converts the signal into the time-frequency domains. For a continuous signal $x(t)$, the wavelet transform is defined as

$$\psi_{a,b}(t) = \frac{1}{\sqrt{a}}\psi\left(\frac{t-b}{a}\right) \quad a > 0,\ b \in R \tag{1}$$

where ψ is the wavelet function, and a and b are the time scale and time shift, respectively. The discrete wavelet function can be defined by using the dyadic grid-sampling method.

And, the dyadic orthogonal wavelet function, $\psi_{m,n}(t)$, can be written as

$$\psi_{m,n}(t) = 2^{-m/2}\psi\left(2^{-m}t - n\right) \tag{2}$$

where m is the parameter of dilation and n is the parameter of position.

Wavelet analysis is a good tool to develop multi-resolution analysis to separate a signal into the low- and high-frequency bands (Morsi and El-Hawary, 2007). As that shown in Fig. 6, a three-layer resolution of a signal is presented. The high- and low-frequency band components are, respectively,

$$c_m[k] = \sum_n c_{m-1}[n]g(n-2k) \tag{3}$$

$$d_m[k] = \sum_n c_{m-1}[n]h(n-2k) \tag{4}$$

where m is the resolution layer, and g and h represent the low- and high-pass filters, respectively.

2. Wavelet Based Stationary-Non-Stationary Filter

Under some operation conditions, the current waveforms of some home appliances have impulse characteristics that can influence the accuracy of serial arc fault detection. Therefore, the WTST-NST is employed to eliminate the impulse components.

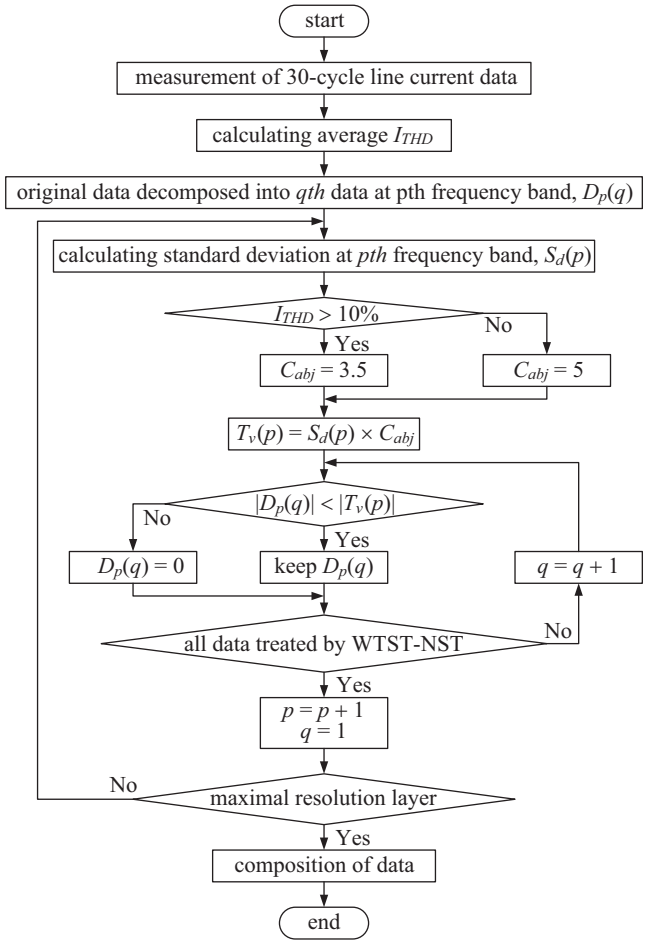

Fig. 7. Procedure of eliminating impulse components by using WTST-NST.

The procedure of WTST-NST is shown in Fig. 7. The 30-cycle line current measurement data are used to calculate the total harmonic distortion (THD) per power cycle by using the Fast Fourier Transform (FFT). The average THD, I_{THD}, of the 30 cycles is obtained. At the second step, the original signal is decomposed to relative frequency bands by using DWT and multi-resolution analysis. The standard deviation of each frequency band is multiplied by a constant, and the product is used as the threshold, which can be described by

$$T_v(p) = S_d(p) \times C_{abj} \tag{5}$$

where $S_d(p)$ is the standard deviation of the pth frequency band, and C_{abj} is used to sustain the threshold at a high value (Hadjileontiadis and Panas, 1997). In this study, we choose $C_{abj} = 3.5$ when $I_{THD} > 10\%$, and $C_{abj} = 5.0$ when $I_{THD} \le 10\%$. At the third step, the data after multi-resolution analysis are compared with a corresponding threshold $T_v(p)$. If the absolute value of the data is higher than the absolute value of the corresponding threshold, the data will be reset to zero; otherwise, the data will be kept.

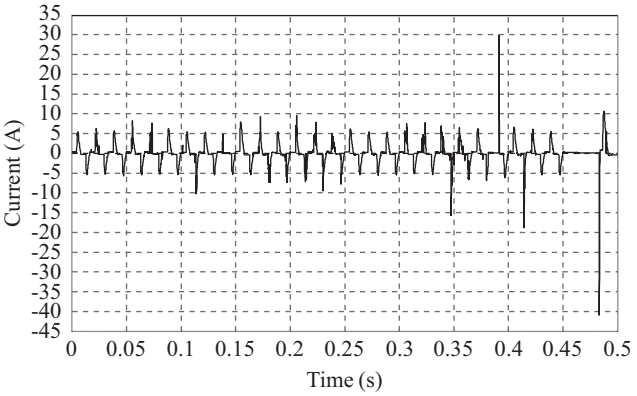

Fig. 8. Original Current waveform of experimental data.

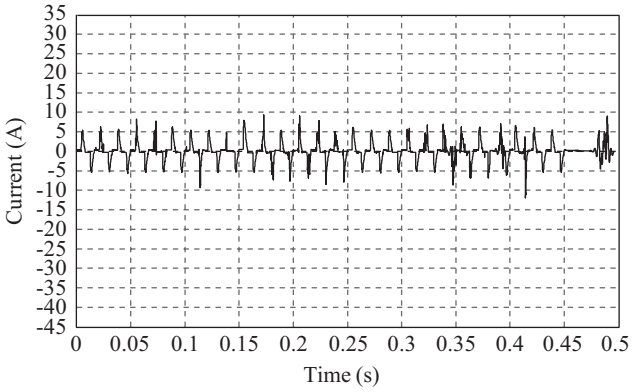

Fig. 9. Current waveform after being eliminated impulse components by using WTST-NST.

By comparing Figs. 8 and 9, it can be observed that the WTST-NST can eliminate the impulse components.

3. Signal Energy

After the measurement data have been treated by WTST-NST, the signal c_0, whose impulse compoents have already been eliminated, can be decomposed into relative frequency band by an N-layer resoulution as

$$c_0 = c_N + d_1 + d_2 + d_3 + \ldots + d_N \tag{6}$$

the signal energy of each high frequency sub-band can be obtained by

$$x_{D_m} = \sum_{k=1}^{H} d_m[k]^2,\ m = 1,\ 2,\ 3,\ \ldots,\ \mathrm{N} \tag{7}$$

where d_m represents the amplitude of the discrete points corresponding to the *mth* layer, and H is the number of data in that layer. The characteristic vectors as the inputs to train the BPNN can be expressed by

$$X = [x_{D_1},\ x_{D_2},\ x_{D_3}, \ldots, x_{D_N}]^t \tag{8}$$

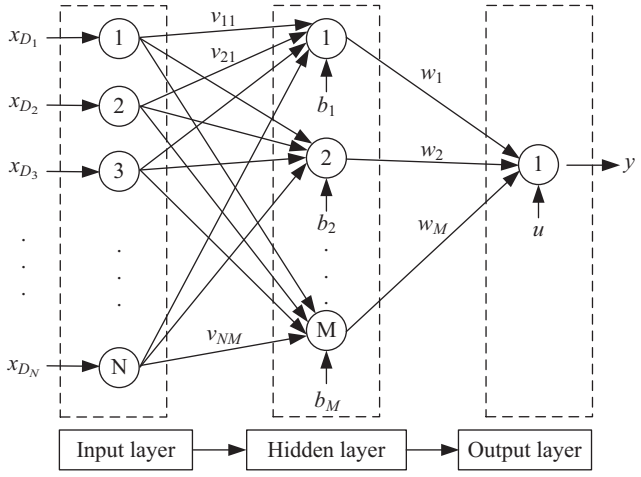

Fig. 10. BPNN structure.

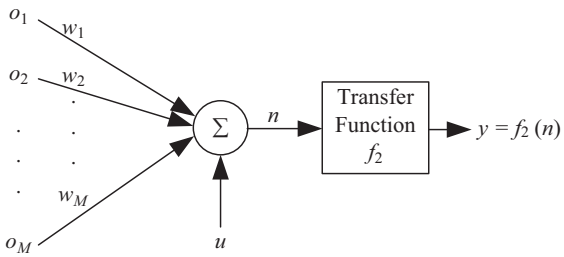

Fig. 11. Relation between hidden layer and output layer.

IV. BACK-PROPAGATION NEWRAL NETWORKS

The BPNN structure is shown in Fig. 10. There are three layers, input, hidden, and output. Each layer has different number of neurons. There are N signal energy values used as the inputs to the BPNN, and there is only one output to reveal whether the serial arc fault occurs or not.

The relation of the neurons in hidden layer and output layer is shown in Fig. 11. The summation is

$$n = \sum_{j=1}^{M} w_j o_j + u \tag{9}$$

where w_j is an weighting value between the *jth* neuron in hidden layer and the neuron in output layer. The u is a bias value of the neuron in output layer. The o_j indicates the output from the *jth* neuron in hidden layer. In this study, the hyperbolic tangent function and the linear function, as shown in Fig. 12, are chosen as the transfer function in hidden layer and output layer, respectively. Thus, the value of the neuron in output layer can be obtained by

$$y = f_2(n) = \sum_{j=1}^{M} w_j o_j + u \tag{10}$$

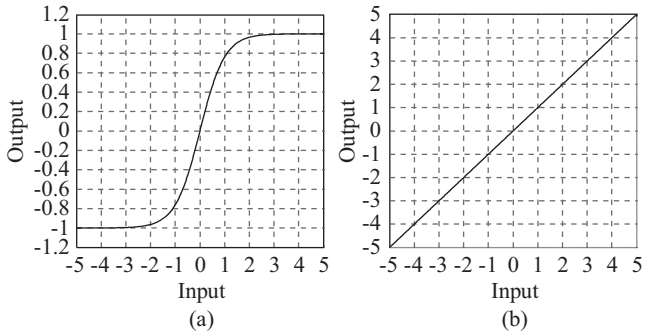

Fig. 12. Characteristic of transfer functions (a) hyperbolic tangent function. (b) linear function.

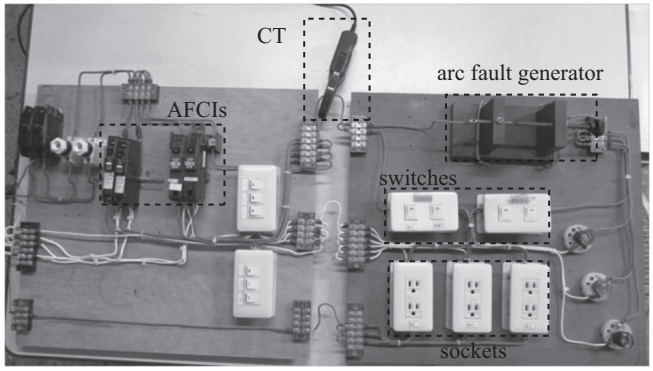

Fig. 13. Experimental circuit.

In the hidden layer, each neuron can get the summation by

$$m_j = \sum_{i=1}^{N} v_{ij} x_{Di} + b_j,\ j = 1, 2, \ldots, M \tag{11}$$

where v_{ij} is an weighting value between the ith neuron in input layer and the jth neuron in hidden layer. The b_j is a bias value of the jth neuron. Therefore, the values of the hidden layer can be represented as

$$o_j = f_1(m_j) = \frac{e^{m_j} - e^{-m_j}}{e^{m_j} + e^{-m_j}},\ j = 1, 2, \ldots, M \tag{12}$$

After all training data have be sent to the BPNN, it can obtain a group of estimated signal $Y(\lambda)$at the λth iteration as

$$Y(\lambda) = [y_1(\lambda)\ \ y_2(\lambda)\ \ \ldots y_R(\lambda)] \tag{13}$$

where R is the total amount of input data. The difference $e(\lambda)$ between the expected signal T and the estimated signal $Y(\lambda)$ at the λth iteration is

$$e(\lambda) = \sum [T - Y(\lambda)] = \sum_{r=1}^{R} [t_r - y_r(\lambda)] \tag{14}$$

The error function to be minimized can then be conveniently defined as

$$E(\lambda) = \sum 0.5 e^2(\lambda) = 0.5 \sum_{r=1}^{R} [t_r - y_r(\lambda)]^2 \tag{15}$$

The gradient descent method is used to update weighting values and bias values, that is,

$$\frac{dE(\lambda)}{dW_j} = 0 \quad \frac{dE(\lambda)}{dU} = 0 \quad \frac{dE(\lambda)}{dV_{ij}} = 0 \quad \frac{dE(\lambda)}{dB_j} = 0 \tag{16}$$

The estimated parameters at the $(\lambda + 1)th$ iteration can be obtained by

$$W_j(\lambda + 1) = W_j(\lambda) + \eta_1 e(\lambda) f_2'(n) O_j \tag{17}$$

$$U(\lambda + 1) = U(\lambda) + \eta_2 e(\lambda) f_2'(n) \tag{18}$$

$$V_{ij}(\lambda + 1) = V_{ij}(\lambda) + \eta_3 e(\lambda) f_2'(n) W_j f_1'(m_j) X_i \tag{19}$$

$$B_j(\lambda + 1) = B_j(\lambda) + \eta_4 e(\lambda) f_2'(n) W_j f_1'(m_j) \tag{20}$$

where η_1 and η_2 are the learning factors for the weighting factors and bias values in the output layer, respectively. The η_3 and η_4 are the learning factors for the weighting factors and bias values in the hidden layer, respectively.

V. TRAINING OF BPNN

The experimental circuit includes an AFCI, an arc generator, switches, and sockets (Fig. 13). A current transformer (CT) is used to measure current waveforms on the power line. The sampling frequency is 20 kHz. To prepare the training data of the BPNN, it should be noted that different electrical appliances have different current characteristics. Then, three loading conditions are considered, that is, (a) a rice cooker (resistive load), (c) a hairdryer (inductive load), and (c) fluorescent lamps (harmonic load).

The sampled data are treated by the WTST-NST to reduce the impulse components. The resulted data are analyzed by the multi-resolution to obtain the sub-band components and the corresponding signal energy. It has been observed that the characteristics of high-frequency bands of the fourth layer change dramatically. Therefore, only the values of signal energy of the first three high-frequency sub-bands are selected as the characteristics to train the BPNN.

The signal energy of the system feeding three loading conditions and under two operation conditions, normal operation, and serial arc fault, respectively, are considered in training the

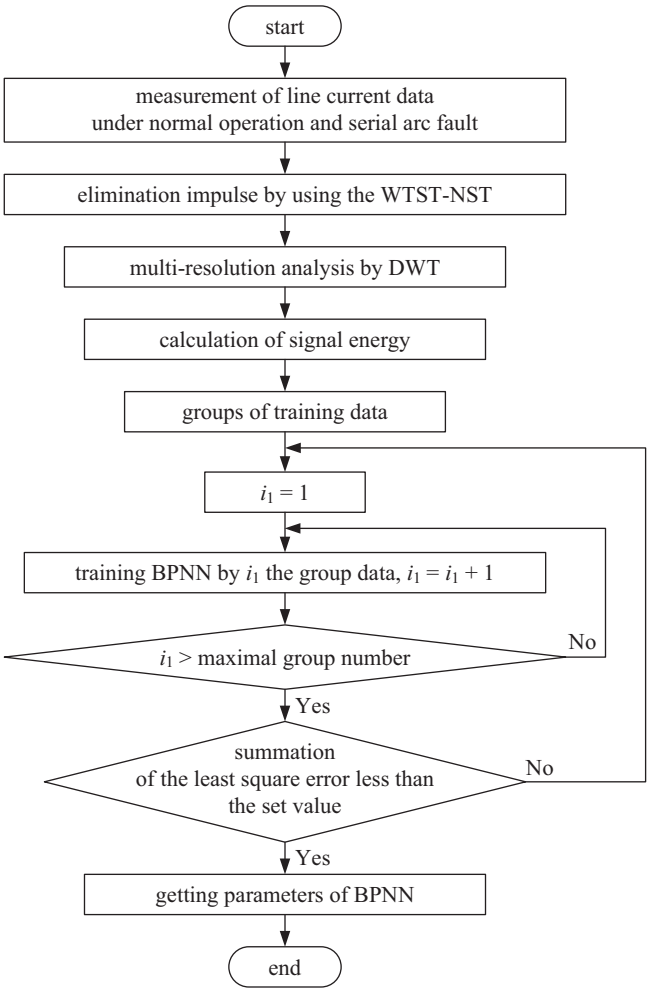

Fig. 14. Training procedure of BPNN.

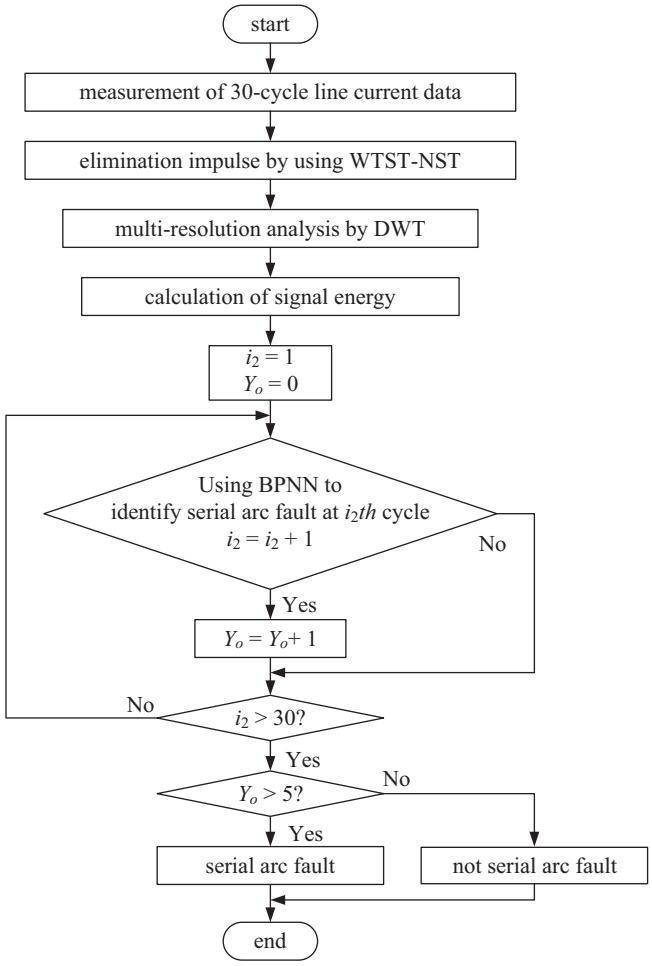

Fig. 15. Procedure of serial arc fault detection by using BPNN.

BPNN. The training procedure of BPNN is shown in Fig. 14. The data of line current within one power cycle can give a group of training data. Therefore, there are totally 60 groups of training data. The output of BPNN is set to "1" if a serial arc fault occurs in that cycle; otherwise, the output of BPNN is "-1." When the summation value of the least square errors is less than the set value, the training process is terminated.

VI. DETECTION RESULTS BY USING BPNN

To examine the detection of serial arc faults by using the BPNN, four loading conditions are employed, which include (a) a rice cooker and a parallel resistor, (b) a hairdryer, (c) fluorescent lamps and a parallel resistor, and (d) a rice cooker, an electric fan, and fluorescent lamps. According to the UL Standard 1699 (Arch-fault circuit interrupters, 2008), the line current should be larger than 5A for an AFCI to detect serial arc faults. Thus, the parallel resistor in some conditions are used to increase the current magnitude.

The procedure of serial arc fault detection by using the BPNN is shown in Fig. 15. In order to consider practical usage of

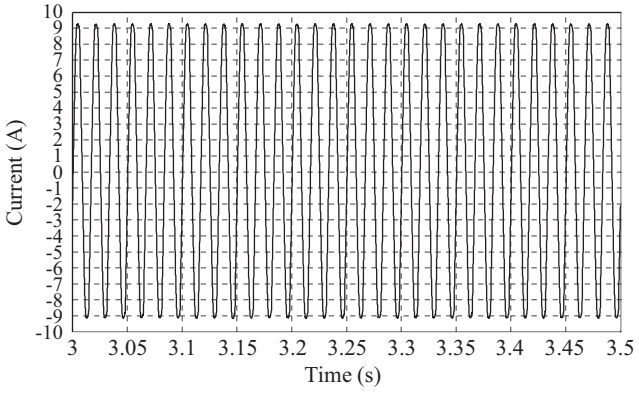

Fig. 16. Current waveform of the system feeding a rice cooker and a parallel resistor under normal operation.

electrical appliances, three operation conditions are considered, normal operation, on/off switching, and serial arc fault. In the detection procedure, the BPNN gives one output for each power cycle. The value is "1" if it identifies that a serial arc fault occurs, and "-1" otherwise. If the total number of "1" within 30 power cycles is greater than 5, the BPNN identifies that a serial

Table 1. Output of BPNN of the system feeding a rice cooker and a parallel resistor under three operation conditions.

cycle number	normal operation	on/off switching	serial arc fault
1	-1	-1	1
2	-1	-1	-1
3	-1	-1	1
4	-1	-1	1
5	-1	-1	1
6	-1	-1	1
7	-1	-1	1
8	-1	-1	1
9	-1	-1	1
10	-1	-1	-1
11	-1	-1	-1
12	-1	-1	-1
13	-1	-1	-1
14	-1	-1	-1
15	-1	-1	-1
16	-1	-1	-1
17	-1	-1	-1
18	-1	-1	-1
19	-1	-1	-1
20	-1	-1	-1
21	-1	-1	-1
22	-1	-1	-1
23	-1	-1	-1
24	-1	-1	-1
25	-1	-1	-1
26	-1	-1	-1
27	-1	-1	-1
28	-1	-1	-1
29	-1	-1	1
30	-1	-1	-1

arc fault has occurred on the power line.

1. A Rice Cooker and a Parallel Resistor

The line current waveforms of the system feeding a rice cooker and a parallel resistor are shown in Figs. 16-18. The 30 outputs of the BPNN are listed in Table 1. From the test result, the BPNN does not gives any "1" for the system under normal operation. Under on/off switching, there is also no "1". Thus, the BPNN identifies correctly that a serial arc fault does not occur under these two conditions. Under a serial arc fault, there are more than five "1" from the BPNN. So, the BPNN identifies correctly that a serial arc fault occurs. However, the commercial AFCI had a mistake and did not shut down the power source for the system under a serial arc fault, as shown in Fig. 18.

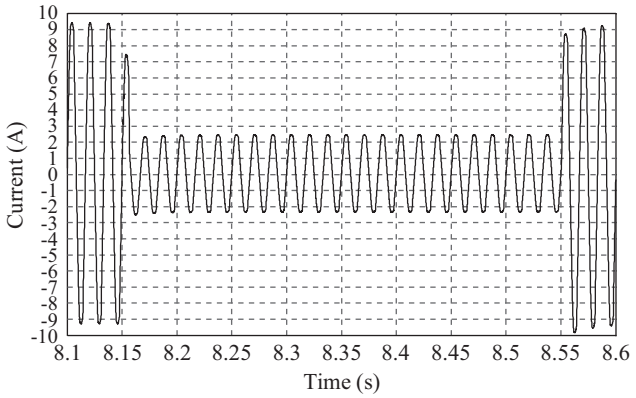

Fig. 17. Current waveform of the system feeding a rice cooker and a parallel resistor under on/off switching.

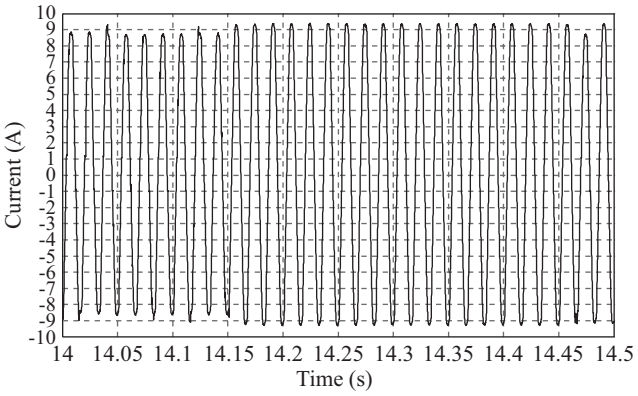

Fig. 18. Current waveform of the system feeding a rice cooker and a parallel resistor under a serial arc fault.

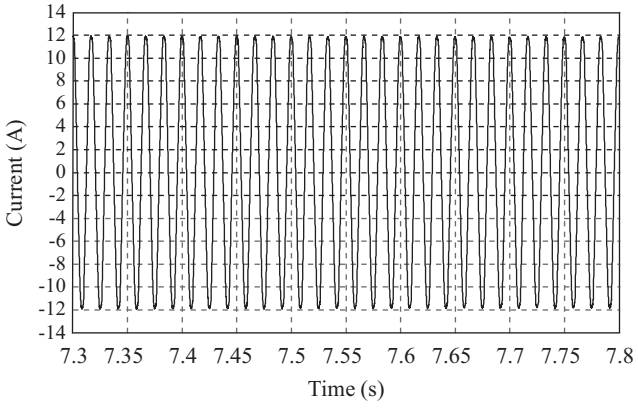

Fig. 19. Current waveform of the system feeding a hairdryer under normal operation.

2. A Hairdryer

The current waveforms of the system feeding a hairdryer are shown in Figs. 19-21. Table 2 gives the 30 output results of the BPNN for the system under three operation conditions, respectively. There is no "1" from the BPNN for the system under normal operation. Under the on/off switching condition,

Table 2. Output of BPNN of the system feeding a hairdryer under three operation conditions.

cycle number	normal operation	on/off switching	serial arc fault
1	-1	-1	1
2	-1	-1	1
3	-1	-1	1
4	-1	-1	1
5	-1	-1	1
6	-1	1	1
7	-1	-1	-1
8	-1	-1	1
9	-1	-1	1
10	-1	-1	1
11	-1	-1	1
12	-1	-1	1
13	-1	-1	1
14	-1	-1	-1
15	-1	-1	1
16	-1	-1	1
17	-1	-1	1
18	-1	-1	1
19	-1	-1	1
20	-1	-1	1
21	-1	-1	1
22	-1	-1	1
23	-1	-1	1
24	-1	-1	1
25	-1	-1	1
26	-1	-1	1
27	-1	-1	1
28	-1	-1	1
29	-1	-1	1
30	-1	-1	1

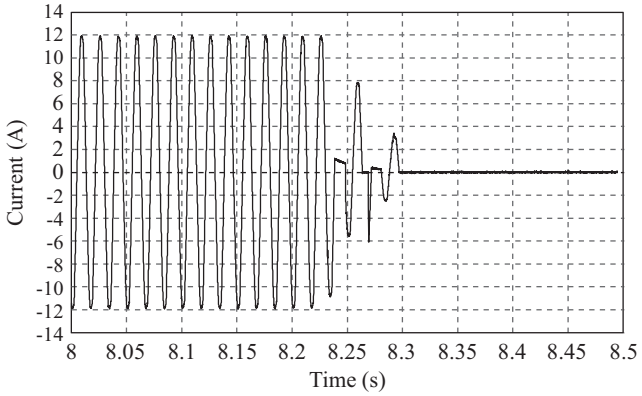

Fig. 20. Current waveform of the system feeding a hairdryer under on/off switching.

the amount of "1" is only 1. Thus, the BPNN identifies correctly that a serial arc fault does not happen under these two operation conditions. However, Fig. 20 shows that the commercial AFCI made a mistake to shut down the power source under the on/off switching condition.

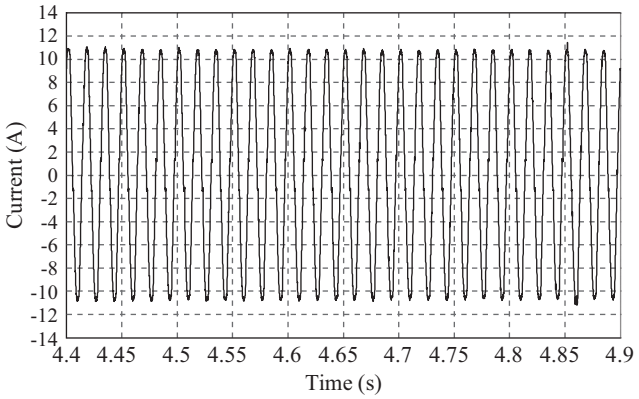

Fig. 21. Current waveform of the system feeding a hairdryer under serial arc fault.

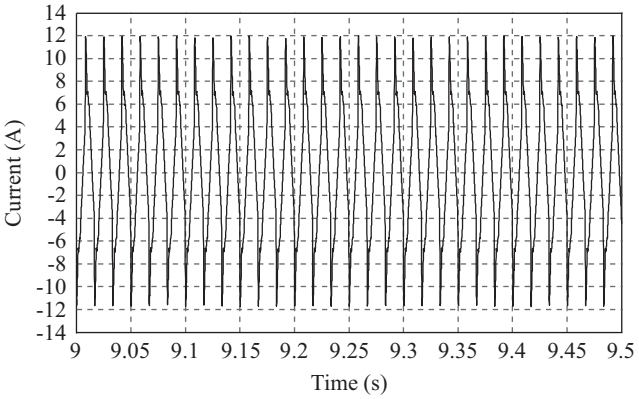

Fig. 22. Current waveform of the system feeding fluorescent lamps and a parallel resistor under normal operation.

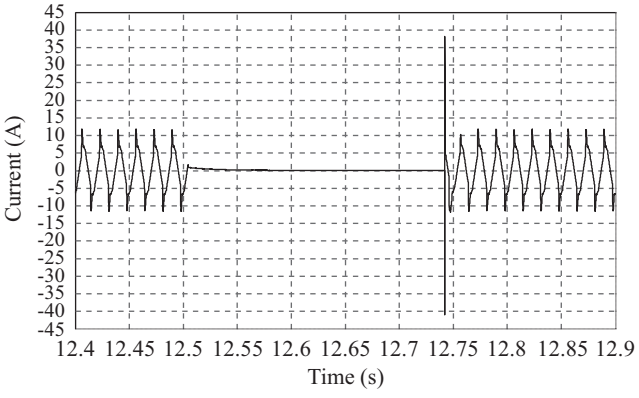

Fig. 23. Current waveform of the system feeding fluorescent lamps and a parallel resistor under on/off switching.

Under a serial arc fault, the "1" appears more than five times within the 30 power cycles, therefore, the BPNN identifies correctly that a serial arc fault occurs. However, as shown in Fig. 21, the commercial AFCI also made a mistake, since it did

Table 3. Output of BPNN of the system feeding fluorescent lamps and a parallel resistor under three operation conditions.

cycle number	normal operation	on/off switching	serial arc fault
1	-1	-1	1
2	-1	-1	1
3	-1	-1	1
4	-1	-1	1
5	-1	-1	-1
6	-1	-1	1
7	-1	-1	-1
8	-1	-1	1
9	-1	-1	1
10	-1	-1	1
11	-1	-1	1
12	-1	-1	1
13	-1	-1	1
14	-1	-1	1
15	-1	-1	-1
16	-1	-1	-1
17	-1	-1	-1
18	-1	-1	1
19	-1	-1	-1
20	-1	-1	-1
21	-1	1	-1
22	-1	-1	-1
23	-1	-1	-1
24	-1	-1	-1
25	-1	-1	-1
26	-1	-1	-1
27	-1	-1	-1
28	-1	-1	-1
29	-1	-1	-1
30	-1	-1	-1

not shut down the power source during the serial arc fault condition.

3. Fluorescent Lamps and a Parallel Resistor

The current waveforms of the system feeding fluorescent lamps and a parallel resistor are shown in Figs. 22-24. The 30 output results of the BPNN are listed in Table 3. By observing the results, no "1" appears at the output of the BPNN for the system under normal operation. Under the on/off switching condition, the amount of "1" is 1. Thus, the BPNN identifies that a serial arc fault does not occur under these two conditions. There are more than five "1" under a serial arc fault condition. Therefore, the BPNN identifies correctly that a serial arc fault occurs in the power line. At this test, the commercial AFCI also acted correctly, since it shut down the power source during the serial arc fault condition.

4. A Rice Cooker, an Electric Fan, and Fluorescent Lamps

The current waveforms of the system feeding a rice cooker, an electric fan, and fluorescent lamps are shown in Figs. 25-27. Table 4 gives the 30 output results of the BPNN under three operation conditions, respectively. The total amount of "1" are 0, 1, and 27, respectively, under normal operation, on/off switching, and a serial arc fault. So, the BPNN identifies correctly that a serial arc fault occurs under a serial arc fault. But by observing

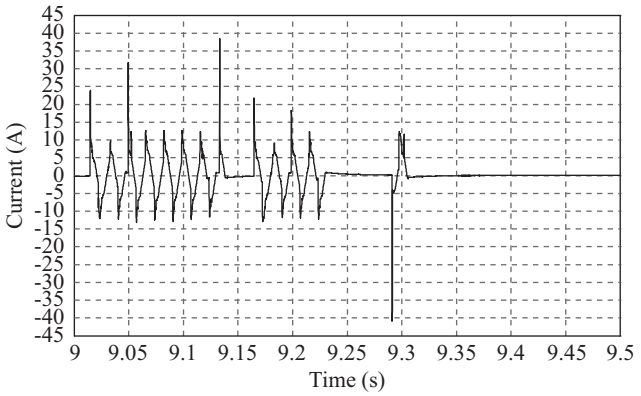

Fig. 24. Current waveform of the system feeding fluorescent lamps and a parallel resistor under serial arc fault.

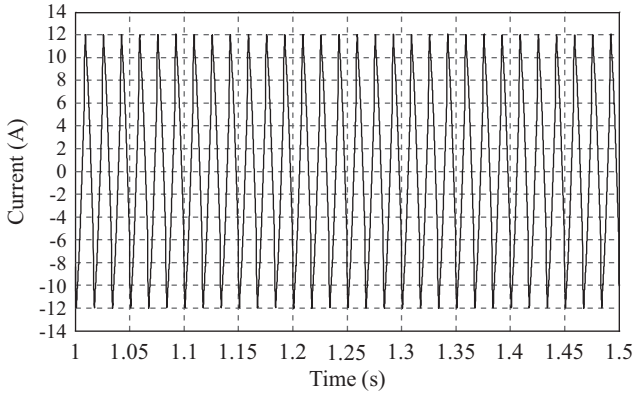

Fig. 25. Current waveform of the system feeding a rice cooker, an electric fan, and fluorescent lamps under normal operation.

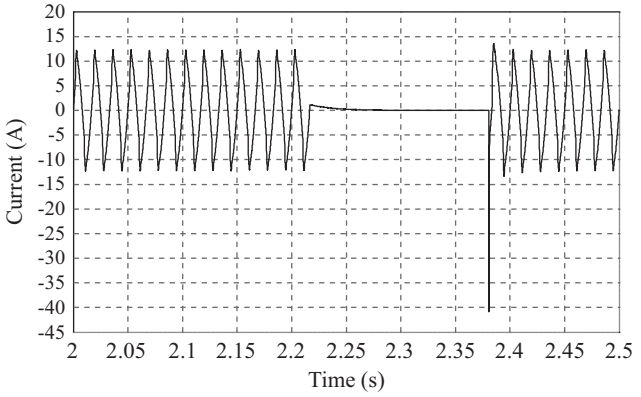

Fig. 26. Current waveform of the system feeding a rice cooker, an electric fan, and fluorescent lamps under on/off switching.

Table 4. Output of BPNN of the system feeding a rice cooker, an electric fan, and fluorescent lamps under three operation conditions.

cycle number	normal operation	on/off switching	serial arc fault
1	-1	-1	-1
2	-1	-1	-1
3	-1	-1	1
4	-1	-1	1
5	-1	-1	1
6	-1	-1	1
7	-1	-1	1
8	-1	-1	1
9	-1	-1	1
10	-1	-1	1
11	-1	-1	1
12	-1	-1	1
13	-1	-1	1
14	-1	-1	-1
15	-1	-1	1
16	-1	-1	1
17	-1	-1	1
18	-1	-1	1
19	-1	-1	1
20	-1	-1	1
21	-1	-1	1
22	-1	-1	1
23	-1	1	1
24	-1	-1	1
25	-1	-1	1
26	-1	-1	1
27	-1	-1	1
28	-1	-1	1
29	-1	-1	1
30	-1	-1	1

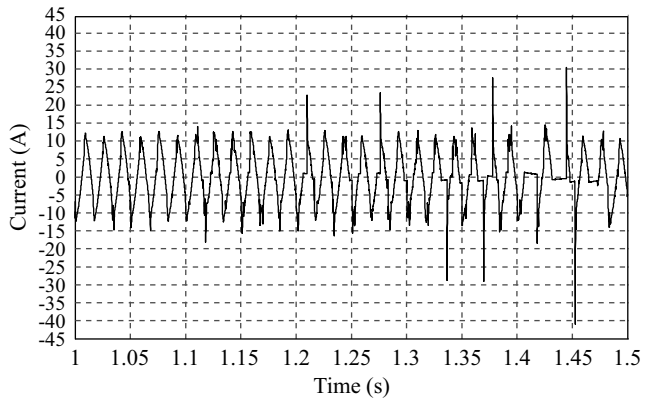

Fig. 27. Current waveform of the system feeding a rice cooker, an electric fan, and fluorescent lamps under serial arc fault.

Fig. 27, the commercial AFCI made a mistake and did not shut down the power source under a serial arc fault.

Table 5. Correctness of serial arc fault detection.

	normal operation		on/off switching		serial arc fault	
	AFCI	BPNN	AFCI	BPNN	AFCI	BPNN
a rice cooker and a parallel resistor	Yes	Yes	Yes	Yes	No	Yes
a hairdryer	Yes	Yes	No	Yes	No	Yes
fluorescent lamps and a parallel resistor	Yes	Yes	Yes	Yes	Yes	Yes
a rice cooker, an electric fan, and fluorescent lamps	Yes	Yes	Yes	Yes	No	Yes

In summary, the comparison of detection results between the commercial AFCI and the purposed method is listed in Table 5. It can be observed that the AFCI has several mistakes, while the purposed method can identify correctly.

VII. CONCLUSIONS

This paper gives a good method to detect the serial arc faults on low voltage electric power lines. The impulse components in the waveforms of line current can be removed by WTST-NST. Then the multi-resolution analysis based on DWT is used to obtain the values of signal energy of corresponding sub-bands, which can be used as the characteristics to train the BPNN, and also used to detect the serial arc faults. Several loading conditions and several operation conditions are considered. This study also compares the test results with a commercial AFCIs. The test results confirm the feasibility of the suggested method.

REFERENCES

Abedi, A (2010). Signal detection in passive wireless sensor networks based on back-propagation neural networks. Published in IET Wireless Sensor Systems 1(1), 48-54.

Arc-fault circuit interrupters, UL Standard 1699-2008 (2008).

Cheng, H., X. Chen, F. Liu and C. Wang (2010). Series arc fault detection and implementation based on the short-time Fourier transform. Proceeding of the 2010 Asia-Pacific Power and Energy Engineering Conference, Chengdu, China, 1-4.

Gregory, G. D. and G. W. Scott (1998). The arc-fault circuit interrupter: an emerging product. IEEE Transaction on Industry Applications 34(5), 928-933.

Gregory, G. D., K. Wong and R. F. Dvorak (2004). More about arc-fault circuit interrupters. IEEE Transaction on Industry Applications 40(4), 1006-1011.

Hadjileontiadis, L. J. and S. M. Panas (1997). Separation of discontinuous adventitious sounds from vesicular sounds using a wavelet-based filter. IEEE Transactions on biomedical engineering 44(12), 1269-1281.

Hall, J. R. (2013). Home structure fires by equipment involved in ignition. National Fire Protection Association Fire Analysis and Research Division, Quincy, Massachusetts, USA, NFPA No. USS87.

Kim, C. H., H. Kim, Y. H. Ko, S. H. Byun, R. Aggarwal and A. T. Johns (2002). A novel fault-detection technique of high-impedance arcing faults in transmission lines using the wavelet transform. IEEE Transaction on Power Delivery 17(4), 921-929.

Koziy, K., B. Gou and J. Aslakson (2013). A low-cost power-quality meter

with series arc-fault detection capability for smart grid. IEEE Transaction on Power Delivery 28(3), 1584-1591.

Lin, Y. H., C. W. Liu and C. S. Chen (2004). A new PMU-based fault detection/location technique for transmission lines with consideration of arcing fault discrimination-part I: theory and algorithms. IEEE Transaction on Power Delivery 19(4), 1587-1593.

Lippert, K. J. and T. Domitrovich (2013). AFCIs – from a standards perspective. Proceeding of the 2013 IEEE IAS Electrical Safety Workshop, Dallas, Texas, USA, 57-61.

Ma, S. and L. Guan (2011). Arc-fault recognition based on BP neural network. Proceeding of the Third International Conference on Measuring Technology and Mechatronics Automation, Shanghai, China, 584-586.

Morsi, W. G. and M. E. El-Hawary (2007). Reformulating power components definitions contained in the IEEE standard 1459-2000 using discrete wavelet transform. IEEE Transaction on Power Delivery 22(3), 1910-1916.

Muller, P., S. Tenbohlen, R. Maier and M. Anheuser (2010). Characteristics of series and parallel low current arc faults in the time and frequency domain. Proceeding of the 56th IEEE Holm Conference on Electrical Contacts, Charleston, South Carolina, USA, 1-7.

Naidu, M., T. J. Schoepf and S. Gopalakrishnan (2006). Arc fault detection scheme for 42-V automotive DC networks using current shunt. IEEE Transaction on Power Electronics 21(3), 633-639.

Su, W. Y. and C. J. Wu (2010). The assessment of introduction of the arc fault circuit interrupters. Institute of Occupational safety and health, Taipei, Taiwan, IOSH98-S302.

Zhang, R. and Z. Song (2012). Arc fault detection method based on signal energy distribution in frequency band. Proceeding of the 2012 Asia Pacific Power and Energy Engineering Conference, Shanghai, China, 1-4.